

CHAPTER 2

EXPERIMENTAL DETAILS

2.1 Introduction

2.2 Particle accelerators

2.2.1 FOTIA, Van-De-Graff, BARC: Construction and working principle

2.2.2 Experimental details of the irradiation done at FOTIA

**2.2.3 Irradiation set-up at six meter height of BARC-TIFR Pelletron:
Construction and working principle**

**2.2.4 Experimental details using irradiation set-up at six meter height of
BARC-TIFR Pelletron**

2.3 Neutron sources

2.3.1 Fission

2.3.2 Neutron sources based on (α ,n) reaction

2.3.3 Neutron sources based on accelerated charged particle

2.3.4 Photo-neutron sources

2.4 Target preparation

2.4.1 Preparation of targets by rolling technique

2.4.2 Preparation of lithium fluoride target by pelletization method

2.4.2 Preparation of lithium target by rolling technique and pressing technique

2.5 Detection and measurement of γ -rays

2.5.1 Nuclear radiation detectors

2.5.2 Semiconductor detectors

2.5.3 Construction and working principle of HPGe Detector

2.5.4 Measurement of γ -ray activity

2.6 Neutron activation technique

2.7 Neutron energy calculation

2.8 Neutron flux calculation

2.9 Reaction cross-section derivation

2.10 Error in the calculation of cross-section

References

2.1 Introduction

Neutron induced reaction cross-sections for the ^{197}Au , ^{55}Mn , ^{232}Th and ^{238}U targets at different neutron energies were measured in the present work. All the experimental facilities used to carry out the present work, are explained in this chapter. Two different accelerators Folded Tandem Ion Accelerator (FOTIA) facility located at Van-De-Graaff at Bhabha Atomic Research Centre (BARC), Mumbai and BARC-TIFR Pelletron Facility located at Tata Institute of Fundamental Research (TIFR), Mumbai were used to generate neutron beam for the present work. All the targets used in the present work were prepared at Radiochemistry Division at BARC, Mumbai and target preparation laboratory at TIFR [1-13]. Two HPGe detectors having different specifications were used for the γ -ray spectrometry [14-15]. The present chapter begins with the brief introduction of particle accelerators: FOTIA and Pelletron with a complete description of the experimental set up related to that. This chapter also includes the different techniques used for the preparation of the targets and detectors, used in the present work. Neutron sources and neutron activation technique followed by a derivation of reaction cross-section [1-12] are also discussed in brief.

2.2 Particle accelerators

For the development of an advanced reactor, charged particle accelerator plays a key role. Students of Lord Rutherford, J. D. Cockcroft and E.T.S. Watlton built a high voltage generator, on the suggestion of Lord Rutherford. It was based on the principle of voltage multiplication, which was first proposed by H. Greinacher (1921). J. D. Cockcroft and E.T.S. Watlton were the first to generate nuclear transmutation with artificially accelerated proton in 1931.

There are mainly two types of accelerators. First type of accelerators is the electrostatic accelerators. Here, constant voltage difference is applied between the target and the ion source and hence, the charged particles are accelerated. The final energy of the particle depends upon the voltage difference. Van-de-Graaff and Cock kroft-walton generators fall in this category. These accelerators have the limitation that they can only accelerate the particles up to a few million electron volts (MeV) as they breakdown because of the discharge between the walls of the accelerator chamber and the high voltage terminal. The second type is known as cyclic accelerators. Here the particle trajectory is curved in the cyclotron, betatron, synchro-cyclotron and synchrotron and straight in the linear accelerator. In the second type accelerators, the charge particles are accelerated in multiple steps, transmitting the small amount of energy in each consecutive step [1, 2, 13].

2.2.1 FOTIA, Van-De-Graff, BARC: Construction and working principle

This machine was developed by R. J. Van de Graff in 1931. In this, the HV is charged by a convective current. An insulating belt is made to rotate on two pulleys P_1 and P_2 by a motor, which is connected with pulley P_2 and is kept to the ground potential. Along the belt, metal points are extended equidistantly at the potential difference of 20-30 kV. When these points are at positive potential, there occurs a corona discharge between the belt and these points, which ionizes the gas. This in turn sprays the positive charge on the moving belt. The pulley P_1 is kept inside a large hollow metal sphere S . Further, another set of sharp corona points is connected to S . They remove the charge of the corona points and pass it on to the later. This charge gets accumulated gradually on the outer sphere surface S . Thus, the potential of the sphere increases gradually. The larger the sphere, the more charge it can hold, which will lead to a very high potential. Top end of the accelerator tube T and ion source are kept inside the HV terminal S . The potential of 1.5 million volt was generated by the first machine built by Van de Graaff, which was accelerating 1.5 MeV energy protons with a beam current of 25 μA [3, 13].

2.2.2 Experimental details of the irradiation done at FOTIA

Sample irradiations for some of the elements used in the present work, were carried out by using the neutron beams at FOTIA (Folded Tandem Ion Accelerator) facility at Nuclear Physics Division in BARC, Mumbai. ${}^7\text{Li}(p,n){}^7\text{Be}$ reaction ($E_{\text{th}}=1.881$ MeV) was used to generate the neutron beam with the help of proton beam. A circular pellet of lithium fluoride (LiF) having 1 cm of diameter and 3 mm of thickness was made by using the LiF powder. It was mounted on a holder at 0° angle relative to the exit window of the beam. In order to focus the beam, a beam collimator having 10 mm diameter was used before the target. Lithium fluoride pellet is sufficient to stop proton beam. Here, we get quasi-mono energetic neutron beam, as the proton beam loses energy in lithium and also in the experimental set up, there happens a finite angular coverage of the neutron capture reaction. Target was wrapped in aluminium foil. A 1 mm thick monitor sample foil of the same size as the target, wrapped separately in 0.025 mm thick 99% pure aluminium foil, was kept with the target. The weight of the aluminium foil in which samples were wrapped, was noted first. Then the weight of the sample along with the aluminium was taken. The subtraction of the aluminium foil from the weight of the samples wrapped in aluminium foil gives the sample weight. Both the targets and flux monitor stacks were of a square shape with 1.0 cm^2 size.

Thus, weights and sizes of both the samples are taken care to minimize the area corrections during the neutron flux calculations. These stacked samples were mounted at 0° with respect to the beam direction at 3 mm distance, behind the LiF pellet. The additional monitor target helps us to know the neutron flux (number of the neutrons coming from the beam to the target per unit area per unit time). These sets of samples were irradiated for fixed time. The incident beam current during all the irradiations was kept constant. All the activated samples were cooled for certain time. After cooling, the irradiated samples were detached carefully with the use of forceps from the holder stand and kept carefully in a lead pot. This lead pot along with the activated samples was taken to the counting room. Then all the samples were mounted one by one on the centre position of different Perspex plates. The mounted samples were kept one at a time on a particular shelf of the sample holder (Perspex stand) attached to an HPGe detector for γ -ray counting [15]. Experimental arrangement is shown in figure 2.1.

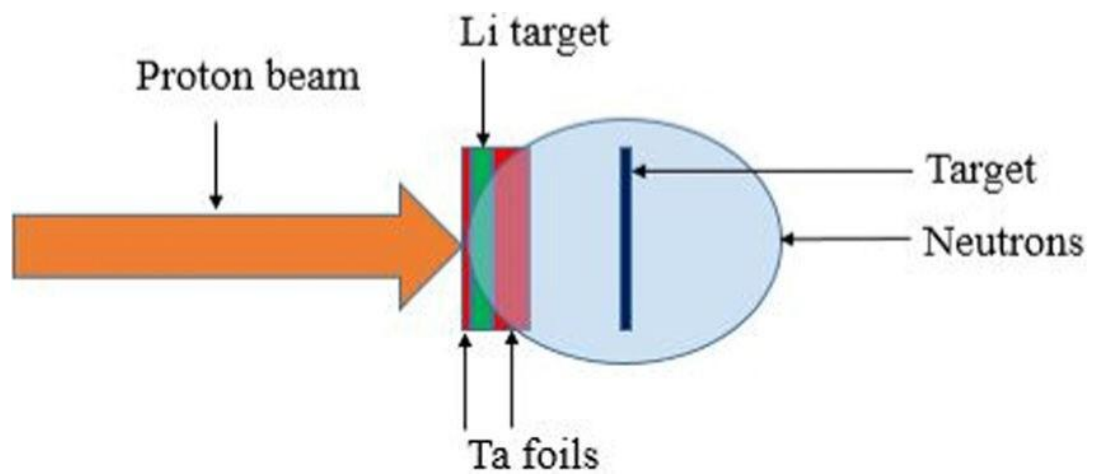


Figure 2.1: Experimental arrangement showing the irradiation set up using the $\text{Li}(p,n)$ reaction neutron source at FOTIA [18]

2.2.3 Irradiation set-up at six meter height of BARC-TIFR Pelletron: Construction and working principle

Design of the charging mechanism is different in Pelletron accelerator. Here, charging chain is used instead of the charging belt. This charging chain has steel cylinders, joined with the insulating material (nylon). As metal cylinders leave the pulley at the ground potential, they are charged. As they pass over a pulley within the high voltage terminal, the charge is removed. Beam current ranges from a few μA to 0.8 mA [7-8].

2.2.4 Experimental details using irradiation set-up at six meter height of BARC-TIFR Pelletron

For sample irradiations in the present work, 14 UD Pelletron facility at BARC-TIFR (Bhabha Atomic Research Centre - Tata Institute of Fundamental Research), Mumbai, India, has also been used. This has been done since the accelerator in FOTIA (BARC) was able to accurately deliver, the proton beams only up to 6 MeV energy [15-16]. On the other hand, in BARC-TIFR Pelletron facility, the proton beam up to 24 MeV energy can be generated based on the terminal voltage of 12 MV. Here, the desired neutron beams were obtained from the ${}^7\text{Li}(p,n){}^7\text{Be}$ reaction, as mentioned above, using proton beams in the main line, 6 m height above the analysing magnet of Pelletron. The 6 meter height port was used for exploiting the maximum proton current from the Pelletron. The broadening of proton beam at 6 meter port was found to be around 50~90 keV. A terminal potential stabilizer was used in order to regulate the terminal voltage by generating voltage mode (GVM). A collimator having 6-mm diameter was used before the target to get circular shaped beam. The lithium metal foil having 3.7 mg/cm^2 thickness was placed between two tantalum plates having different thicknesses. The thinnest tantalum foil of 3.9 mg/cm^2 thickness faces the proton beam (front tantalum). The degradation of the proton energy in the front Ta foil was estimated by using the SRIM code [17] and was found to be around 30 keV. In order to stop the proton beam, the thickness of the back tantalum foil was kept 6.66 mg/cm^2 (0.025 mm). The generated quasi mono-energetic neutrons were used to irradiate the samples. The sample targets were wrapped in the 99% pure Al foil having the thickness of 0.025 mm. Similarly, the monitor sample was also wrapped in 0.025 mm thick aluminium foil, separately. Both the target and monitor foils were again packed in a common aluminium foil. Sizes of both the samples were kept the same (1.0 cm^2) in order to avoid the area corrections. They were separately wrapped with Al foils separately so that the reaction products can be stopped from recoiling out from the surface of the samples and collected easily. As described in reference [15], samples were

mounted behind the Ta–Li–Ta stack at a distance of 2.1 cm at an angle of 0° with respect to the beam direction. Proton beam was bombarded on Ta–Li–Ta stack and the neutron beam will be emitted. Samples were irradiated with neutron beam for particular time. The proton current was kept constant throughout the irradiation. Activated samples were cooled for specific time. After cooling the samples, they were mounted in the centre of different Perspex plates with the help of a forceps. The mounted samples were kept one at a time on a particular shelf of sample holder (Perspex stand) attached to an HPGE detector for γ -ray counting. The distance of the sample from the detector head was kept 5 cm for all the measurements. The arrangement for the irradiation is shown in the below figure 2.2.

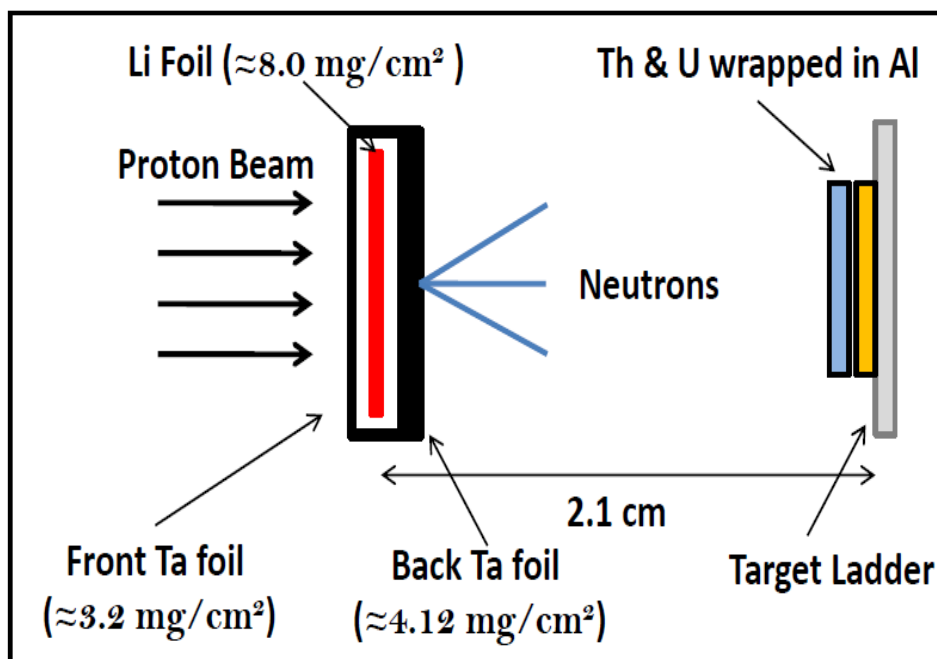


Figure 2.2: Experimental arrangement showing the neutron production using the ${}^7\text{Li}(p, n)$ reaction using Pelletron facility at TIFR

2.3 Neutron sources

Neutrons are emitted as a result of different nuclear reactions. There are several examples of such nuclear reactions, some of them are given below:

2.3.1 Fission

This reaction is one of the most common neutron source. During the nuclear fission, fast neutrons are produced. Spontaneous fission of ^{252}Cf is one of such fission neutron source.

2.3.2 Neutron sources based on (α ,n) reaction

$^{241}\text{Am} + ^9\text{Be}$ is one of the good example of (α ,n) neutron source. Here alpha particle emitted from the ^{241}Am react with ^9Be to produce neutron. The $^{241}\text{Am} + ^9\text{Be}$ neutron source can be used for long time due to the 432.6 y half-life of ^{241}Am .

2.3.3 Neutron sources based on accelerated charged particle

These sources are used when highly intense beams of mono-energetic neutrons are needed. Accelerated light particles like proton, deuteron and α - particle from the accelerator are bombarded on deuteron, triton, $^{\text{nat}}\text{Li}$ or ^9Be target which will produce mono-energetic or quasi-mono energetic neutrons. Among all these, the D+D and D+T reactions produced mono-energetic neutrons of 2.45 and 14.8 MeV, respectively [16].

In some of the cases, particle will break the target nuclei (break up reaction) and this nuclear reaction will no longer be the two-body reaction. In some cases, primary neutrons will interact with the structural material. In such cases, secondary (background) neutrons will be produced along with the primary (foreground) neutrons. Therefore, mono-energetic neutron beam will not be possible but a neutron spectrum having a sharp peak corresponding to primary reaction and a tail part due to secondary reaction is usually produced.

Mono energetic neutron beam possibility depends on the intensity of the charged particle beam falling on the target nuclei, thickness of target, differential cross-section of the nuclear reaction and specific energy loss in the target. In order to achieve high specific yield, one must have a high neutron production cross-section as well as minimum energy loss of the incident particles in the target material. In present work I have used $^7\text{Li}(p,n)^7\text{Be}$ reaction for the generation of neutron beam by using the FOTIA at Van-de-graff building at BARC or the BARC-TIFR Pelletron facilities at TIFR, Mumbai. The Q-value of $^7\text{Li}(p,n)^7\text{Be}$ reaction is - 1.644 MeV, whereas the threshold energy is 1.881 MeV.

2.3.4 Photo-neutron sources

These sources can be generated by using photon beam. Photon beams are generally bombarded on the deuteron or ^9Be isotopes. This reaction is endoergic. Therefore, the energy of the incident particle should be greater than the threshold energy. The threshold energy for the $^2\text{H}(\gamma, n)$ reaction is 2.26 MeV and that of $^9\text{Be}(\gamma, n)$ reaction is 1.66 MeV. These reactions have greater possibility of the generation of mono-energetic neutron beam. On the other hand, neutron beam with spectrum of energy can be produced by bombarding the bremsstrahlung (spectrum of photon) on a series of tantalum or tungsten target. The bremsstrahlung is usually produced by injecting the electron beam from a LINAC on the first tantalum or tungsten target. The bremsstrahlung spectrum also carries the end-point energy of the electron. The neutron produced from such facility is commonly used for time-of-flight (TOF) experiments to determine the resonance reaction cross-sections.

2.4 Target preparation

Almost all the targets were provided by Dr. H. Naik from Radio Chemistry Division, and Dr. Y. Nayak from Product Development Division of BARC. Some of the targets were not in the desired shape, therefore appropriate techniques were used to get the desired shape of the targets, which are discussed in the sections 2.4.1, 2.4.2 and 2.4.3.

2.4.1 Preparation of targets by rolling technique

Some of the targets used in the present work were prepared by Rolling Technique at target laboratory located at Tata Institute of Fundamental Research. The desired target was kept between two Teflon plates having dimensions of 50 mm x 50 mm x 0.7/0.8 mm and rolled for 2-3 times. After that, the direction of target foil was altered and rolled again for 2-3 times. Then it was cut into a square shape. This target piece was weighed and the thickness was calculated. Then its area was measured and noted down. This procedure was repeated until the desired thickness of target foil was achieved. Figure 2.3 shows the rolling mill which was used for the preparation of target samples.

Some of the targets in the present work were used in the powder form. First, the aluminium foil (0.025 mm thick) was weighed with the help of digital weighing machine. After that, the powder sample was wrapped inside the aluminium foil. This foil along with the powder sample was weighed. By subtracting the aluminium foil's weight from the weight of aluminium foil having powder sample inside it, one can get the weight of the powder sample.

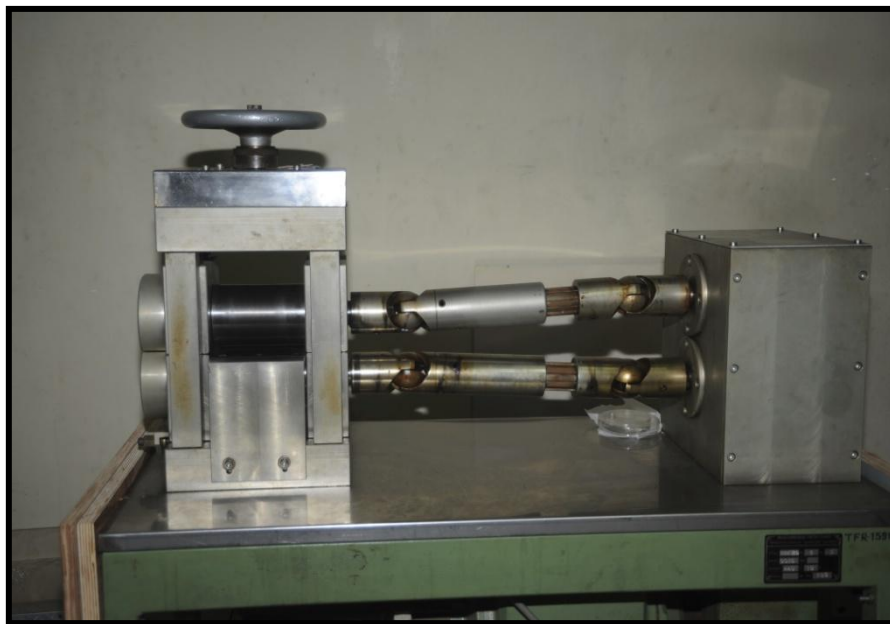


Figure 2.3: Rolling mill at target laboratory, BARC-TIFR Pelletron facility, Mumbai

2.4.2 Preparation of lithium fluoride target by pelletization method

Pelletizing is a sample preparation method, in which spherical and flat pellets are made out of powder sample. In this method, agglomeration of fine, amorphous powder is done with the help of a pelletizer. Some of the lithium targets used in the present work were prepared by pelletizer at target preparation lab at Product Development Division, BARC. Raw lithium fluoride (LiF) powder was fed continuously into the pelletizer and pellets were ejected from the edge of the rotating drum. The pelletizer used in the present work is shown in the figure 2.4.

2.4.3 Preparation of lithium target by rolling technique and pressing technique

The Lithium metal foil, which was used for generating neutron beam with the help of proton beam was prepared by Rolling Technique at target laboratory located at Tata Institute of Fundamental Research. The foil was kept in liquids like kerosene or paraffin oil. Before the use, it was cleaned with tissue paper watchfully. After that, the procedure as explained in the section 2.4.1 was repeated for gaining the desired shape and thickness of the lithium target.

2.5 Detection and measurement of γ - rays

Most of the radioactive materials produce γ -rays, with different energies and different intensities, which decides the unknown isotope of an element. Because of the nuclear reactions, the reaction product decays to excited states of the daughter nucleus, which de-excites in order to get the stability back with the emission of radiation, generally with the emission of γ -rays. If these γ -rays, which are emitted by the product nuclei, are detected and studied in details with a spectroscopy system, there will be a γ -ray energy spectrum. By studying the γ -ray spectroscopy, one is enabled towards learning the characteristics of the substance more in terms of depth. Spectrometry is a critical tool for the identification of the nuclides. The amplitude of the spectrum lines from the γ -ray spectrometry is directly proportional to the nuclide activity. Spectrum line position on the horizontal axis provides the idea of the energy of the nuclide. Nuclear radiation detection plays most crucial role in unfolding the mysteries of atomic nucleus. Emitted radiation carries important information about nucleus. Therefore, their detection and measurement is mandatory for understanding the structure of the nucleus and nuclear reactions [13-14, 18-21]. Figure 2.5 shows the typical set up used for γ -ray spectroscopy.



Figure 2.4: Pelletizer, used for making Lithium pellets

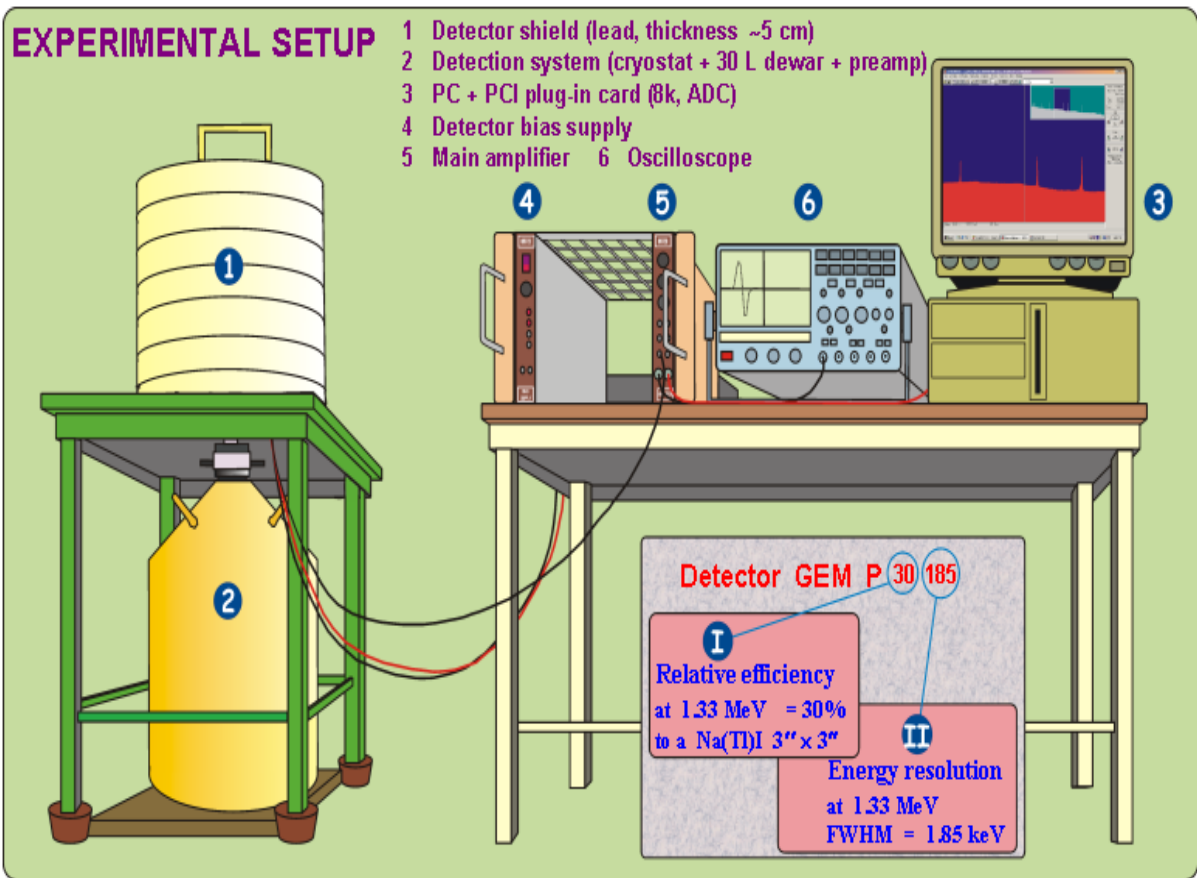


Figure 2.5: Typical set up used for γ -ray spectroscopy

2.5.1 Nuclear radiation detectors

Radiation detectors are the devices that are used for detecting the radiation like α , β or γ -rays. Earlier, the detection of the nuclear radiation was done by simple detecting devices. These devices are now replaced by more efficient and advanced devices. Some of these detectors are based on the ionization chamber, proportional counter, Geiger-Muller counter, semiconductor detector. Some detectors are based on light sensing like scintillation detector, Cherenkov detectors etc. Some are based on the method of visualization of the track of ionizing radiation like Wilson cloud chamber. Spark chamber, bubble chamber, diffusion cloud chamber, bubble chamber, cloud chamber, nuclear emulsion technique [13-14, 18-21].

2.5.2 Semi-conductor detectors

These devices work on the principle of direct collection of the charge produced because of the interaction of the γ -ray with the material. An arrangement where cadmium sulphide or diamond crystal is kept between two electrodes and both the electrodes are kept at a large potential difference, is known as a semi-conductor device. These kinds of devices can detect high-energy radiation. Semi-conductor detectors are reverse biased junction diodes. They offer better energy resolution and fast response for the incident radiation. These devices use silicon or germanium semiconductor for measuring the effect of incident particles or photons. Semi-conductor detectors are kind of semiconductor diodes, with p-i-n structure. Here, i-intrinsic region is sensitive to ionizing radiation, especially for γ -rays and x-rays applications. Semiconductor detectors are used for radiation protection, γ -ray spectrometry, x-ray spectrometry and particle detection.

2.5.3 Construction and working principle of HPGe detectors

Lithium drifted Ge detector was introduced by A. J. Tavendale and G. T. Ewan in 1962 [14]. It became inevitable part of the γ -ray spectrometry. In HPGe detectors, high purity germanium is used as an intrinsic material for the depletion region. This material is kept between two electrodes. When the radiation strikes the depletion region, it forms the electron-hole pair. The generation of number of electron-hole pair will depend upon the energy and intensity of the incident radiation. Because of this, a number of electrons are transported to the conduction band from the valence band and equal number of holes will be created in the valence band. When electric field is applied, electrons travel towards +ve electrode and holes travel towards -ve electrode.

2.5.4 Measurement of γ -ray activity

After the irradiation and sufficient cooling, the target and flux monitor stack was transferred to the counting room. One of the two detectors used for counting of the γ -rays of fission/reaction products from the irradiated samples, used in the present work, was an ORTEC GMX (Model number: GMX 20-70-5) HPGe detector kept at the counting laboratory in RCD, TIFR, Mumbai as shown in the figure 2.6. Before starting the counting process, the energy and efficiency calibration was done for the 80 cm³ HPGe detector, which was attached to a PC-based 4K channel analyzer. The GMX (GAMMA-x) is an N-type Ge crystal that has an ultra-thin entrance window. The thickness of the entrance window is approximately 500 to 100 μ m. During the counting of the samples, the resolution of the detector was measured to be 2.0 keV FWHM at the photo-peak of 1332 keV γ -ray of at 1332 keV of ⁶⁰Co. Activated samples were kept at a certain distance from the detector head for avoiding the pileup effects, which makes the counting dead time of the detector, less than 2%. The standard ¹⁵²Eu multi γ -ray source was used for the energy and the efficiency calibration of the detector system. Typical nature of the detector efficiency is shown in the figure 2.7.



Figure 2.6: ORTEC GMX (Model number: GMX 20-70-5) HPGe detector

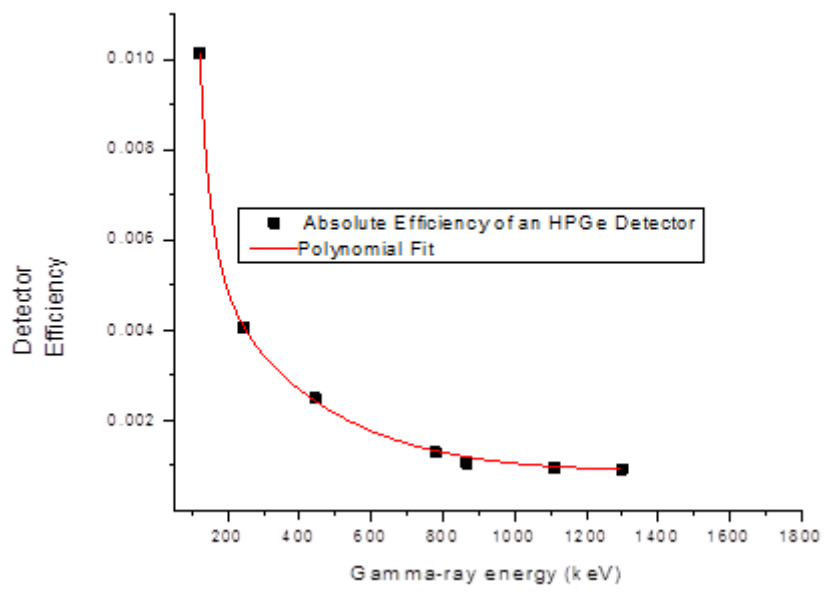


Figure 2.7: Typical characteristic of detector efficiency

According to the half-life of the irradiated samples, the γ -ray counting of the activated samples was repeated over an extended period for reducing the statistical error.

The other detector used in the present work was a Bruker Baltic detector (GCD-20 180) which is a coaxial P-type HPGe detector.

2.6 Neutron activation technique

Neutron activation technique is a powerful tool to determine trace elements, major-minor actinides. It is quite helpful in knowing the concentration of the isotope and is helpful in finding different isotopes in a sample, both qualitatively and quantitatively. It was first established by G. Hevesy and H. Levi [21]. They found that when particular rare earth sample is exposed to a neutron source, the sample gain activity. Detecting and measuring the emitted γ -rays from radioactive isotopes, which were formed by the irradiation of neutrons on the stable isotope (radiative capture), is the principle of neutron activation technique. This technique is non-destructive and it does not demand specific form of the sample. One can apply this technique on any physical form of a sample [22]. In addition, the small amount of the sample is sufficient for this technique. It is based on nuclear reactions and therefore is chemically independent.

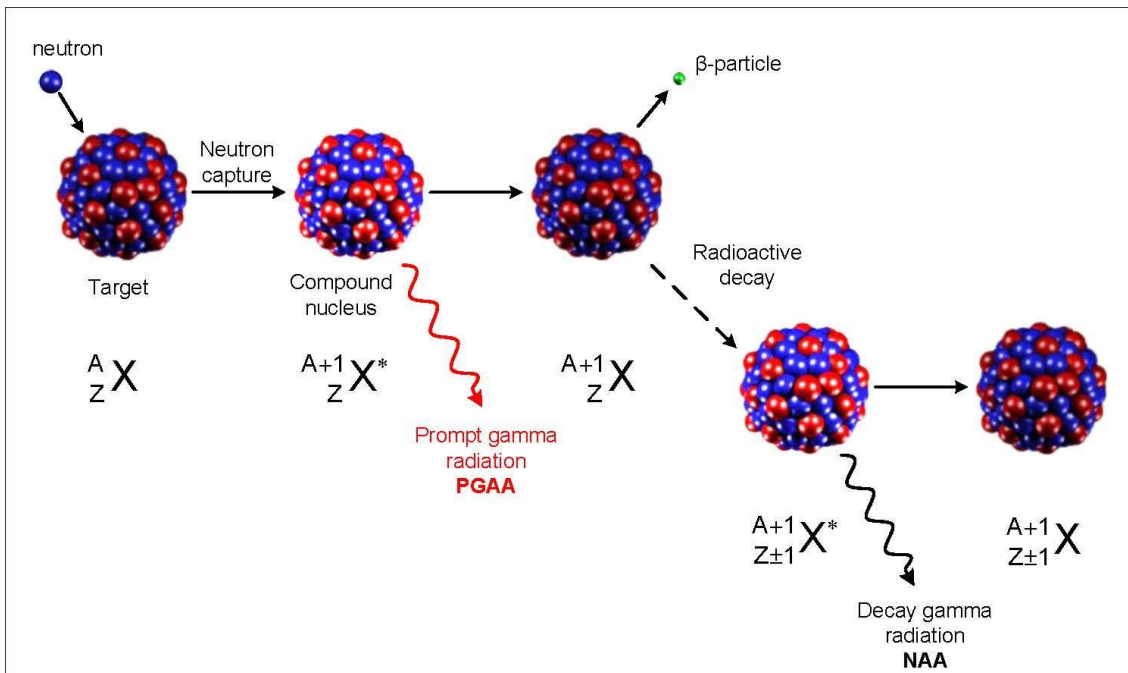


Figure 2.8: Schematic diagram of neutron activation technique

In this technique, sample is activated by neutron beam. Activated natural stable isotopes are transmuted into radioactive isotopes by the interaction of neutrons. This activated sample will decay as per its characteristic half-life, varying from a few seconds to years. Emission of particle and/ or characteristic γ -rays will depend on the energy acquired by the radio-nuclides. The process occurring in neutron activation technique is demonstrated in figure 2.8. Thus, with the help of the characteristic γ -rays, one can get the information regarding the activated sample. For knowing the isotope's radioactivity, high-resolution HPGe detector is used [22-27].

2.7 Neutron energy calculations

Averaged neutron energy of a spectrum is calculated by the following equation [28-30]:

$$E_{\text{mean}} = \frac{\int_{E_{\text{ps}}}^{E_{\text{max}}} E_i \phi_i dE}{\int_{E_{\text{ps}}}^{E_{\text{max}}} \phi_i dE} \quad (2.1)$$

Where, E_{ps} = starting point of energy peak

E_{max} = maximum neutron energy

E_i = Energy bin

Φ_i = Neutron flux associated with energy bin E_i

E_{mean} = effective mean energy

Energies from the starting point of an energy peak (E_{ps}) to the ending point of the energy peak (E_{max}) are taken into account for the calculations of average neutron peak energy and respective neutron production flux (ϕ_i) with possible average bins. Multiplication of E_i and ϕ_i is integrated over E_{ps} and E_{max} and is divided by the integration of total ϕ_i over E_{ps} and E_{max} . This will give E_{mean} , averaged energy value.

Neutron spectra related to the present work were generated with the help of Monte Carlo N-Particle code (MCNP), which was run by Dr. Mohamad Zaman of Korea and Dr. Karel Katovski from Berno.

2.8 Neutron flux calculation

Monitor is an additional target, kept along with the main target, which helps us to determine the number of neutrons falling on the target's square meter or centimetre area per second. Neutron induced reaction cross-section of the flux monitor must be previously known accurately, in order to calculate the neutron flux precisely. The precision in the calculation of the neutron flux will decide the accuracy of the cross-section of the main target. Thus,

choosing a flux monitor requires rigorous exercise as the accuracy of cross-section of the target depends on the accuracy maintained in flux measurement.

Spectrum averaged neutron cross-section data were taken from EXFOR [16] data library, which enabled us to calculate the neutron flux incident on the target. The spectrum-averaged flux was calculated by the following equation:

$$\Phi_{av} = \frac{\int_{E_{th}}^{E_{max}} \sigma_i \phi_i dE}{\int_{E_{th}}^{E_{max}} \sigma_i dE} \quad (2.2)$$

Where, E_{th} = threshold energy of the monitor reaction

E_{max} = Neutron's maximum energy

σ_i = cross-section at energy E_i for monitor reaction from monitor

Φ_i = Neutron flux associated with energy bin E_i

σ_{av} = spectrum averaged cross-section

The neutron flux incident on all the targets was calculated with the help of the following equation:

$$\Phi = \frac{A_\gamma \lambda (t_c / t_r)}{N \sigma_{av} I_\gamma \varepsilon (1 - e^{-\lambda t_i})(1 - e^{-\lambda t_c}) e^{-\lambda t_w}} \quad (2.3)$$

Where, A_γ = Number of detected γ -rays

λ = Decay constant of the product nucleus

t_c = Counting time

t_r = Real time clock time (sec)

N = Number of atoms in target

σ = cross-section of monitor reaction

I_γ = Branching intensity of γ -ray

ε = Efficiency of the detector for the chosen γ -ray

t_i = Irradiation time (sec)

t_w = Cooling time (sec)

To determine N (total number of atoms present in the target), following equation was used.

$$N = \frac{N_0 \times \text{Sample weight} \times \text{Isotopic abundance}}{\text{Isotopic Mass}} \quad (2.4)$$

Here, N_0 = Avogadro number = 6.023×10^{23}

2.9 Reaction cross-section derivation

Reaction cross-section is a probability for a nuclear reaction to occur. If the measured cross-section contains all the possible interactions, it is the total cross-section parallel with the reaction cross-sections. There also exists scattering of two types: 1) elastic and 2)

inelastic scattering. Cross-sections are measured in the units of area and denoted with the help of the symbol σ (sigma).

$$\sigma_{\text{total}} = \sigma_{\text{reaction}} + \sigma_{\text{scattering}} \quad (2.5)$$

A neutron induced reaction especially neutron absorption does not require any threshold energy whereas, for other than capture reactions, the value of threshold energy is non-zero. The threshold value of a reaction falls in MeV range because the nucleus also has binding energy in MeV region. If $E_n > E_{th}$, the reaction rate can be given as follows:

$$R = N \cdot \sigma \cdot \phi \quad (2.6)$$

The reaction rate depends on the cross-section of the given reaction, neutron flux and energy of neutrons [24]. Hence, the activation equation will be written as,

$$R = N \int_0^{\infty} \sigma(E) \phi(E) dE \quad (2.7)$$

Where, R=Reaction Rate

N= No. of target atoms taking part in interaction

$\sigma(E)$ =Cross-section

$\phi(E)$ =Neutron flux

This equation is valid for mono-energetic neutrons only. For quasi-mono energetic neutrons and neutrons having a full spectrum of different neutron energies, the following equation is taken into account [25].

$$R = \int N \cdot \sigma(E_i) \cdot \phi E_{\text{max}} E_{\text{th}}(E_i) dE \quad (2.8)$$

If isotope A gets transmuted into isotope B after the irradiation of isotope A by neutrons. The isotope B further decays to isotope C. This process can be written as follows:



A will produce B but at the same time it will also produce some other isotope through another reaction channels. Isotope B further decays into C and therefore the overall reaction rate for the generation of isotope B can be written as follows:

$$R_b = N_a(t) \sigma_a \phi - N_b(t) \sigma_b \phi - \lambda_b N_b(t) \quad (2.10)$$

$$dN_b/dt = N_a(t) \sigma_a \phi - N_b(t) \sigma_b \phi - \lambda_b N_b(t) \quad (2.11)$$

Where, R_b = reaction rate,

$N_a(t)$ = number of targets of isotope A at time t,

N_b = number of atoms of nuclei B at time t,

The solution of this reaction is given as follow:

$$A_b = N_b(t) \lambda_b = \frac{N_a(0) \sigma_a \phi}{1 + (\sigma_a - \sigma_b) \phi / \lambda_b} [\exp(-\sigma_a \phi t_i) - \exp(-(\lambda_b + \sigma_b \phi) t_i)] \quad (2.12)$$

During the irradiation, very small fraction of the target is destroyed, which is negligible ($\sigma_a \phi t_i \ll 1$). Also, the target must be following the condition of $\lambda_b \gg \sigma_b \phi$. After the application of these conditions, the simplified solution can be written as

$$A_b(t_i) = N_a(0) \sigma_a \phi [1 - e^{-\lambda_b t_i}] \quad (2.13)$$

This formulism is useful in the measurement of neutron flux and/or reaction cross-sections. Irradiation time is denoted as t_i . The radioactivity generated in the target after the irradiation is measured with the help of γ -ray spectrometer. The time gap between the time when irradiation is stopped and counting is started is known as cooling time. Counting time is denoted by T_c and real time is denoted by T_r . Now if the activated sample is counted between time t_1 and t_2 , the reaction cross-section can be given by the following equation:

$$\int A_b(t) dt = \frac{N_a(0) \sigma_a \phi}{\lambda_b} [1 - e^{-\lambda_b t_i}] [e^{-\lambda_b t_1} - e^{-\lambda_b t_2}] \quad (2.14)$$

A_γ is measured activity by γ -ray spectroscopy,

$$A_\gamma = \frac{N_a(0) \sigma_a \phi}{\lambda_b} [1 - e^{-\lambda_b t_i}] [e^{-\lambda_b t_1} - e^{-\lambda_b t_2}] \quad (2.15)$$

$$\sigma_a = \frac{A_\gamma \lambda_b}{N_a(0) \phi [1 - e^{-\lambda_b t_i}] [e^{-\lambda_b t_1} - e^{-\lambda_b t_2}]} \quad (2.16)$$

If the time when counting is started is considered as zero then,

$$\sigma_a = \frac{A_\gamma \lambda_b}{N_a(0) \phi [1 - e^{-\lambda_b t_i}] [1 - e^{-\lambda_b t_c}]} \quad (2.17)$$

Isotope B keeps on decaying even when it is getting cooled so the correction of the cooling time must be applied,

$$\sigma_a = \frac{A_\gamma \lambda_b}{N_a(0) \phi [1 - e^{-\lambda_b t_i}] [1 - e^{-\lambda_b t_c}] e^{-\lambda_b t_w}} \quad (2.18)$$

Including the detector parameter γ -efficiency (ϵ), γ -abundance and time correction, the modified activation formula is now,

$$\sigma_a = \frac{A_\gamma \lambda_b (t_c/t_r)}{N_a(0) \phi I_\gamma \epsilon [1 - e^{-\lambda_b t_i}] [1 - e^{-\lambda_b t_c}] e^{-\lambda_b t_w}} \quad (2.19)$$

The following equation is modified version of the above equation, which is used for the calculation of the cross-sections in the present work.

$$\sigma_R = \frac{A_{obs} \left(\frac{CL}{LT}\right) \lambda}{N \phi I_\gamma \epsilon (1 - \exp[-\lambda t]) \times \exp[-\lambda T] \times (1 - \exp(-\lambda CL))} \quad (2.20)$$

Barn is a standard unit for measuring the cross-section.

$$\begin{aligned} 1 \text{ barn} &= 10^{-28} \text{ m}^2 \\ &= 10^{-24} \text{ cm}^2 \end{aligned}$$

2.10 Error in the calculation of the cross-section

This section briefly describes the methods used for the calculation of the error present in the measured cross-section data of the present thesis. In the present work, the uncertainty in the data can be due to two kinds of errors. One is due to systematic error and the other is due to random errors. Systematic error is because of the uncertainty present in the abundance, detector efficiency, cross-section and hence in neutron flux. Counting statistic causes the random error.

For some of the data in the present work, co-variance analysis was done for the measurement of error, which is discussed and demonstrated in the chapter 6.

References:

- [1] B. R. Martin, Nuclear and Particle Physics, Second Edition, John Wiley & Sons, Ltd. (2006).
- [2] P. E. Hodgson, E. Gadioli and Erba E. Gadioli Ch-4: Particle accelerators and neutron sources, Introductory Nuclear Physics. Clarendon Press-08-28. Oxford (1997).
- [3] S. K. Sahoo, A. K. Rath, R. N. Mukharjee and B. Mallick, Commissioning of a Modern LINAC for Clinical Treatment and Material Research. International Journal of Trends in Interdisciplinary Studies **1**: 10 (2012).
- [4] F. Hinterberger, Electrostatic accelerators (2006).
- [5] D. A. Bromley, The Development of electrostatic accelerators, Nuclear Instruments and Methods **122**: 1-34 (1974).
- [6] O. Sala, Development of electrostatic accelerators, Nuclear instruments and methods in physics research A **280**: 263-269 (1989).
- [7] Tata Institute of Fundamental Research. <http://www.tifr.res.in/~pell/pelletron.html>
- [8] R. P. Sharma, 14 UD Pelletron Accelerator Project at TIFR, Nuclear Instruments and methods in physics research A **244**: 52-53 (1986).
- [9] R. Hellborg, Electrostatic Accelerators: Fundamentals and Applications, Springer Science & Business Media (2006).
- [10] R. Wideroe, Progenitor of Particle Accelerators, SSCL-SR-1186 (1992).
- [11] F. Gerigk, Cavity types. Ar Xiv preprint ar Xiv:**1111**, 4897 (2011).
- [12] V. T. Nimje, D. Bhattacharjee, K. Dixit, D. Jayaprakash, K. C. Mittal and A. K. Ray, Design and development of 30 MeV 3KW, RF electron linac. Asian particle accelerator conference, APAC 491-493 (2007).
- [13] G. F. Knoll, Radiation Detection and Measurement. 3rd Addition, John Wiley and Sons, New York (2000).
- [14] A. J. Tavendale and G. T. Ewan, A High Resolution Lithium-Drift Germanium Gamma-Ray Spectrometer, Nuclear Instruments and Methods **25**: 185-187 (1963).
- [15] V. Vansola, R. Ghosh, S. Badwar, B. M. Lawriniang, A. Gopalakrishna, H. Naik, Y. Naik, N. S. Tawade, S. C. Sharma, J. P. Bhatt, S. K. Gupta, S. Sarode, S. Mukherjee, N. L. Singh, P. Singh, A. Goswami, Radiochim. Acta **103**, 817 (2015).
- [16] EXFOR National Nuclear Data Center, Brookhaven National Laboratory, <http://www.nndc.bnl.gov/exfor>.
- [17] J. F. Ziegler: SRIM-2003. Nucl. Instru. Methods Phys. Res. B **1027**, 219–220 (2004), Available at <http://www.srim.org/>

- [18] D. Reilly, N. Ensslin, H. Smith Jr. And S. Kreiner, Passive Non-destructive Assay of Nuclear Materials (No. NUREG/CR-5550; LA-UR--90-732), Nuclear Regulatory Commission, Washington, DC (United States), Office of Nuclear Regulatory Research; Los Alamos National Lab., NM (United States) (1991).
- [19] P. Sangsingkeow, K. D. Berry, E. J. Dumas, T. W. Raudorf and T. A. Underwood, Advances in Germanium Detector Technology, Nuclear Instruments and Methods in Physics Research Section A. **505**, 183-186 (2003).
- [20] Y. Mei-Woo, Determination Performance of Gamma Spectrometry Co-Axial HPGE Detector In Radiochemistry And Environment Group, Nuclear Malaysia (2014).
- [21] G. Hevesy and H. Levi, Math Fys Medd **14**, 34 (1936).
- [22] Overview of Neutron Activation Analysis Hosted Online by The University of Missouri Research Reactor, < <http://archaeometry.missouri.edu/naaoverview.html> >
- [23] Z. B. Alfassi, Activation Analysis, Volumes I and II. CRC Press: Boca Raton, FL (1990).
- [24] Cezar Ciprian Negoita, “Measurement of Neutron Flux Spectra in a Tungsten Benchmark by Neutron Foil Activation Method” 26 (1973).
https://inis.iaea.org/search/search.aspx?orig_q=RN:36065997
- [25] D. De Soete, R. Gijbels and J. Hoste, Neutron Activation Analysis, John Wiley and Sons: New York, NY (1972).
- [26] C. C. Negoita, thesis on “Measurement of Neutron Flux Spectra in a Tungsten Benchmark by Neutron Foil Activation Method”(1973).
- [27] D. B. Syme et al., Fusion Engineering and Design **89**, 2766 (2014).
- [28] C. H. Poppe, J. D. Anderson, J. C. Davis, S. M. Grimes, and C. Wong, Phys. Rev. C **14**, 438 (1976).
- [29] J. D. Anderson, C. Wong, and V. A. Madsen, Phys. Rev. Letts. **24**, 1074 (1970).
- [30] D. L. Smith, et al., “Corrections for Low Energy Neutrons by Spectral Indexing”, Retrieved from: <https://www.oecdnea.org/science/docs/2005/nsc-wpec-doc2005-357.pdf>